

HealthMamba: An Uncertainty-aware Spatiotemporal Graph State Space Model for Effective and Reliable Healthcare Facility Visit Prediction

Dahai Yu¹, Lin Jiang¹, Rongchao Xu¹, Guang Wang^{1*}

¹Florida State University, Tallahassee, Florida, USA
 {dahai.yu, lin.jiang, rxu, guang}@fsu.edu

Abstract

Healthcare facility visit prediction is essential for optimizing healthcare resource allocation and informing public health policy. Despite advanced machine learning methods being employed for better prediction performance, existing works usually formulate this task as a time-series forecasting problem without considering the intrinsic spatial dependencies of different types of healthcare facilities, and they also fail to provide reliable predictions under abnormal situations such as public emergencies. To advance existing research, we propose HealthMamba, an uncertainty-aware spatiotemporal framework for accurate and reliable healthcare facility visit prediction. HealthMamba comprises three key components: (i) a Unified Spatiotemporal Context Encoder that fuses heterogeneous static and dynamic information, (ii) a novel Graph State Space Model called Graph-Mamba for hierarchical spatiotemporal modeling, and (iii) a comprehensive uncertainty quantification module integrating three uncertainty quantification mechanisms for reliable prediction. We evaluate HealthMamba on four large-scale real-world datasets from California, New York, Texas, and Florida. Results show HealthMamba achieves around 6.0% improvement in prediction accuracy and 3.5% improvement in uncertainty quantification over state-of-the-art baselines.

1 Introduction

Healthcare facilities encompass a wide range of locations providing healthcare services, from small clinics and physicians' offices to urgent care centers and large hospitals. They are indispensable to population well-being for preventing and treating disease, enabling continuous care, and forming the backbone of resilient public health systems. Consequently, predicting population visits to healthcare facilities is critical for resource allocation and policy planning [Zhang *et al.*, 2022; Xu *et al.*, 2023; Marcusson *et al.*, 2020].

*Prof. Guang Wang is the corresponding author.

Recent studies on healthcare facility visit prediction have made progress by using statistical methods [Pun *et al.*, 2019; Alghamdi *et al.*, 2019], deep learning methods [Brossard *et al.*, 2025; Karsanti *et al.*, 2019; Salinas *et al.*, 2020; Lim *et al.*, 2021; Li *et al.*, 2022; Piccialli *et al.*, 2020; Zhong *et al.*, 2026], and hybrid approaches [Tuominen *et al.*, 2024; Tang *et al.*, 2023; Skianis *et al.*, 2023]. However, there are three key limitations of existing work. First, prior studies predominantly focus on aggregated visit prediction, overlooking fine-grained healthcare facility types such as ambulatory clinics, hospitals, nursing facilities, and social assistance providers. Second, most existing work formulates healthcare facility visit prediction as a purely time-series forecasting problem, neglecting spatial dependencies that could provide critical information for accurate prediction. Third, most state-of-the-art approaches fail to deliver reliable predictions under public health emergencies and extreme weather events, such as the COVID-19 pandemic and hurricanes.

Hence, in this paper, we aim to develop an uncertainty-aware spatiotemporal framework for type-specific healthcare facility visit prediction that explicitly models spatial dependencies while providing reliable uncertainty estimates. However, there are two key challenges to achieving this. The first challenge lies in the heterogeneity and sensitivity of health-related mobility. Our data analysis indicates that healthcare facility visits exhibit a strong correlation with population structure (e.g., age composition), spatial accessibility, and service availability. These characteristics lead to highly uneven visit patterns across regions and facility types, making it difficult for existing models to capture fine-grained spatiotemporal heterogeneity. Second, reliable uncertainty quantification under abnormal situations remains challenging. During public emergencies such as pandemics, healthcare facility visit behaviors and demand distributions shift dramatically. Without explicit uncertainty modeling, predictions become overconfident and unreliable, potentially leading to misguided decision-making.

To address the above challenges and advance existing research, we propose HealthMamba, which comprises three key components: (i) a **Unified SpatioTemporal Context Encoder (STCE)**, which fuses heterogeneous static and time-varying contextual information and historical visit data into compact node-time representations, (ii) a novel **Graph-Mamba Backbone (G-Mamba)**, which innovatively inte-

grates adaptive graph learning into a UNet-style Mamba architecture for hierarchical spatiotemporal modeling, and (iii) a **comprehensive uncertainty quantification (UQ)** module integrating node-based, distribution-based, and parameter-based UQ mechanisms, followed by a post-hoc quantile calibration to achieve higher prediction reliability.

The key contributions of this paper are as follows:

- **Conceptually**, unlike existing works that focus on aggregated healthcare facility visit prediction and treat this task as a time-series forecasting problem, we target type-specific healthcare facility visit prediction and formulate it as an uncertainty-aware spatiotemporal forecasting task with explicit spatial modeling.
- **Technically**, we propose HealthMamba, an uncertainty-aware spatiotemporal framework comprising three novel components: (i) a Unified Spatiotemporal Context Encoder for heterogeneous information fusion, (ii) a graph state space model called GraphMamba for hierarchical spatiotemporal modeling, and (iii) a comprehensive UQ module that integrates three different UQ mechanisms and a quantile calibration for reliable prediction.
- **Empirically**, we evaluate HealthMamba on four real-world datasets from California, New York, Texas, and Florida by comparing it with 13 state-of-the-art baselines across five metrics. Extensive results demonstrate that HealthMamba achieves 6.0% higher prediction accuracy and 3.5% better uncertainty quantification than the best baseline. Our implementation is available at <https://anonymous.4open.science/r/HealthMamba>.

2 Problem Formulation

Based on data analysis using real-world data, we found that there is a disparity in healthcare facility distribution and accessibility among different regions. For example, there are fewer healthcare facilities in rural areas, and rural residents need to travel longer distances to visit healthcare facilities. In addition, the visit patterns of different types of healthcare facilities are also different. Hence, we intuitively build graphs to model spatial dependencies to predict multi-type healthcare facility visits.

2.1 Spatiotemporal Graph Construction

We define a spatiotemporal graph $\mathcal{G} = (\mathcal{V}, \mathcal{E}, \mathbf{A})$, where $\mathcal{V} = \{v_1, \dots, v_N\}$ denotes N nodes (e.g., counties), \mathcal{E} is the edge set, and $\mathbf{A} \in \mathbb{R}^{N \times N}$ is the weighted adjacency matrix. At each time step t , node i has a feature vector $\mathbf{v}_{i,t} \in \mathbb{R}^C$ representing visit counts across C healthcare facility categories. We construct \mathbf{A} using a Gaussian kernel with sparsity thresholding:

$$a_{ij} = \begin{cases} \exp(-d_{ij}^2/\sigma^2), & i \neq j \text{ and } \exp(-d_{ij}^2/\sigma^2) \geq \epsilon, \\ 0, & \text{otherwise,} \end{cases} \quad (1)$$

where d_{ij} is the centroid distance between nodes v_i and v_j , $\sigma > 0$ controls spatial decay, and $\epsilon \in [0, 1]$ is a sparsity threshold that removes weak connections.

2.2 Healthcare Facility Visit Prediction

Let $\mathbf{V} \in \mathbb{R}^{N \times T_{\text{in}} \times C}$ denote the input visit tensor including features of all N nodes over T_{in} historical time steps across C healthcare facility types. In addition to historical visits, we also incorporate static attributes $\mathbf{D} \in \mathbb{R}^{N \times d_{\text{dem}}}$ (e.g., demographics) and time-varying external factors $\mathbf{E} \in \mathbb{R}^{N \times T_{\text{in}} \times d_{\text{ext}}}$ (e.g., weather, accessibility) as auxiliary inputs, where d_{dem} and d_{ext} denote the dimensions of demographic attributes and external factors, respectively. The goal of healthcare facility visit prediction is to predict future visits for the next T_{out} steps given historical observations and auxiliary information.

Deterministic Prediction

Conventional deterministic prediction learns a mapping f from inputs to point forecasts:

$$\{\mathbf{V}, \mathbf{D}, \mathbf{E}, \mathbf{A}\} \xrightarrow{f} \hat{\mathbf{Y}} \in \mathbb{R}^{N \times T_{\text{out}} \times C}. \quad (2)$$

Probabilistic Prediction

In this work, we focus on probabilistic prediction, which quantifies uncertainty using prediction intervals. Given a target miscoverage rate α (e.g., $\alpha = 0.1$ for 90% coverage), we predict lower, upper, and median quantiles:

$$\{\mathbf{V}, \mathbf{D}, \mathbf{E}, \mathbf{A}\} \xrightarrow{\mathcal{F}} [\hat{\mathbf{L}}, \hat{\mathbf{U}}, \hat{\mathbf{M}}], \quad (3)$$

where $\hat{\mathbf{L}} = \hat{q}_{\alpha/2}(\mathbf{V})$, $\hat{\mathbf{U}} = \hat{q}_{1-\alpha/2}(\mathbf{V})$, and $\hat{\mathbf{M}} = \hat{q}_{0.5}(\mathbf{V})$ represent the lower bound, upper bound, and median predictions, respectively, all in $\mathbb{R}^{N \times T_{\text{out}} \times C}$. The median $\hat{\mathbf{M}}$ also serves as the point prediction, analogous to $\hat{\mathbf{Y}}$ in Eq. (2).

3 Methodology

In this paper, we propose HealthMamba, a spatiotemporal framework for effective and reliable healthcare facility visit prediction. An overview of HealthMamba is shown in Figure 1, which comprises three key components: (i) a **Unified SpatioTemporal Context Encoder (STCE)**, which fuses heterogeneous contextual information and historical visit data into compact node-time representations, (ii) a novel **Graph-Mamba Backbone (G-Mamba)**, which innovatively integrates adaptive graph learning into a UNet-style Mamba architecture for hierarchical spatiotemporal modeling, and (iii) a **comprehensive uncertainty quantification** module integrating node-based, distribution-based, and parameter-based uncertainty quantification, followed by a post-hoc quantile calibration to achieve higher prediction reliability.

3.1 Unified Spatiotemporal Context Encoder

Given the input visit tensor \mathbf{V} , static attributes \mathbf{D} , dynamic external factors \mathbf{E} , and the adjacency matrix \mathbf{A} as defined in Section 2, STCE produces a unified node-time representation $\mathbf{R} \in \mathbb{R}^{N \times T_{\text{in}} \times d_{\text{model}}}$ that fuses these heterogeneous inputs while considering spatial structure and temporal dynamics:

$$\mathbf{R} = \text{STCE}(\mathbf{V}, \mathbf{D}, \mathbf{E}, \mathbf{A}). \quad (4)$$

We utilize d_{hid} and d_{model} to denote the hidden-layer dimension and model output embedding dimension, respectively.

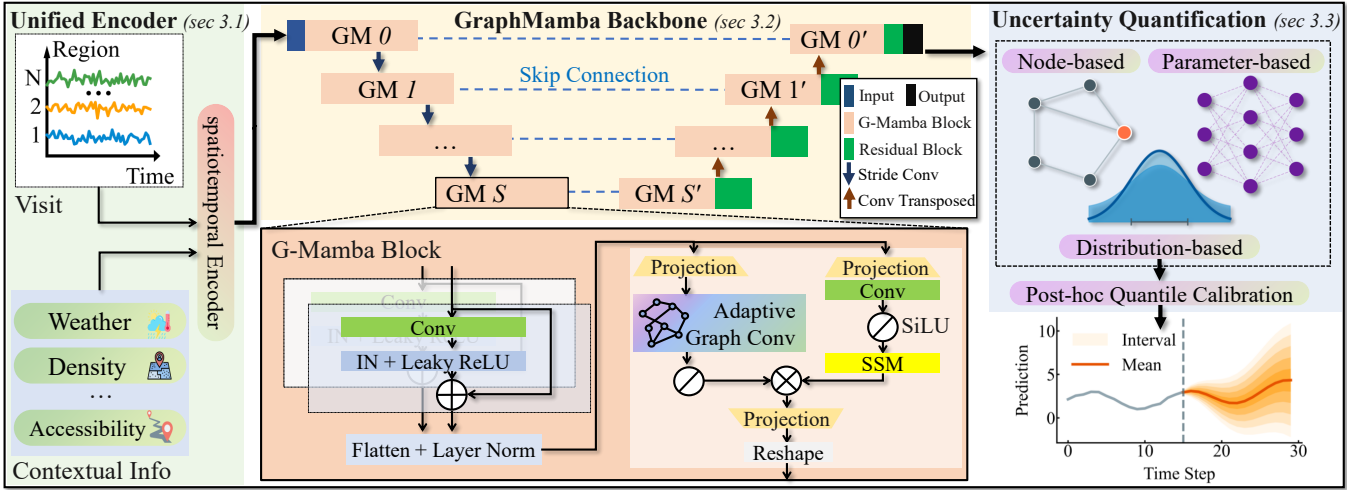


Figure 1: Framework of HealthMamba, which consists of three major components: (i) Unified Spatiotemporal Context Encoder for heterogeneous input fusion, (ii) GraphMamba Backbone for hierarchical spatiotemporal modeling with adaptive graph learning, and (iii) comprehensive uncertainty quantification (UQ) module with three types of UQ mechanisms and post-hoc quantile calibration for reliable prediction.

Specifically, we first map inputs to a common hidden space via feature embedding layers:

$$\mathbf{H}_{i,t}^v = \phi_v(W_v \mathbf{v}_{i,t} + b_v) \in \mathbb{R}^{d_{\text{hid}}}, \quad (5)$$

$$\mathbf{H}_i^d = \phi_d(W_d \mathbf{D}_i + b_d) \in \mathbb{R}^{d_{\text{hid}}}, \quad (6)$$

$$\mathbf{H}_{i,t}^e = \phi_e(W_e \mathbf{E}_{i,t} + b_e) \in \mathbb{R}^{d_{\text{hid}}}, \quad (7)$$

where ϕ_* denotes a nonlinear function (e.g., SiLU/GELU) with dropout. The initial fused embedding at each (i, t) is:

$$\mathbf{X}_{i,t} = \mathbf{H}_{i,t}^v + \mathbf{H}_i^d + \mathbf{H}_{i,t}^e. \quad (8)$$

For spatial encoding, we apply graph convolution with activation function ReLU on node features $\mathbf{X}_{:,t}$ at each time t :

$$\tilde{\mathbf{X}}_{:,t} = \text{GConv}(\mathbf{X}_{:,t}; \mathbf{A}) = \sigma\left(\sum_{j=1}^N \tilde{a}_{ij} W_g \mathbf{X}_{j,t} + b_g\right). \quad (9)$$

For temporal encoding, we mix information across the T_{in} steps for each node i using a light-weight temporal mixer combining depthwise 1D convolution and channel mixing:

$$\mathbf{U}_{i,:} = \text{DepthConv1D}(\tilde{\mathbf{X}}_{i,:}) + \tilde{\mathbf{X}}_{i,:} \in \mathbb{R}^{T_{\text{in}} \times d_{\text{hid}}}, \quad (10)$$

$$\widehat{\mathbf{X}}_{i,t} = \text{MLP}_{\text{chan}}(\text{LayerNorm}(\mathbf{U}_{i,t})) + \mathbf{U}_{i,t}, \quad (11)$$

where DepthConv1D mixes information across the temporal axis and MLP_{chan} performs channel mixing. LayerNorm and residual connections stabilize training. The final projection is:

$$\mathbf{Z}_{i,t} = \text{LayerNorm}\left(W_p [\widehat{\mathbf{X}}_{i,t}; \mathbf{H}_i^d] + b_p\right), \quad (12)$$

$$\mathbf{R}_{i,t} = \text{Dropout}\left(\text{SiLU}(W_o \mathbf{Z}_{i,t} + b_o)\right) \in \mathbb{R}^{d_{\text{model}}}. \quad (13)$$

The encoder output $\mathbf{R} \in \mathbb{R}^{N \times T_{\text{in}} \times d_{\text{model}}}$ serves as the input to the GraphMamba backbone.

3.2 GraphMamba Backbone

In this part, we innovatively integrate an adaptive graph learning module into a UNet-style Mamba architecture for hierarchical spatiotemporal modeling. The input feature at scale s is $\mathbf{X}^{(s)} \in \mathbb{R}^{N \times T_{\text{in}} \times d_s}$, with $\mathbf{X}^{(0)} = \mathbf{R}$. The encoder applies a sequence of G-Mamba blocks followed by downsampling; the decoder performs symmetric upsampling followed by additional G-Mamba blocks. At the coarsest scale, we initialize the decoder by setting $\mathbf{Z}^{(S)} = \mathbf{Y}^{(S)}$. For other scales, we use the following equations.

$$\mathbf{Y}^{(s)} = \text{G-Mamba}^{(s)}(\mathbf{X}^{(s)}), \quad (14)$$

$$\mathbf{X}^{(s+1)} = \text{DownConv}(\mathbf{Y}^{(s)}), \quad s = 0, \dots, S-1, \quad (15)$$

$$\widehat{\mathbf{Y}}^{(s)} = \text{UpConv}(\mathbf{Z}^{(s+1)}), \quad s = S-1, \dots, 0, \quad (16)$$

$$\mathbf{Z}^{(s)} = \text{Fuse}(\mathbf{Y}^{(s)}, \widehat{\mathbf{Y}}^{(s)}). \quad (17)$$

Here, DownConv denotes stride convolution, UpConv denotes transposed convolution, and Fuse represents skip-connection fusion. Each scale maintains its own G-Mamba block without shared weights, allowing scale-specific modeling capacity. The overall algorithm is in Algorithm 2.

G-Mamba Block

Each GraphMamba Block (G-Mamba) is designed to capture spatial dependencies, temporal dynamics, and channel interactions, incorporating an Adaptive Graph Learning mechanism that learns scale-specific, data-driven graph structures.

Adaptive Graph Learning. We first derive a node-level embedding by aggregating temporal information:

$$\mathbf{u}_i = \text{Pooling}(\mathbf{X}_{i,:}^{(s)}). \quad (18)$$

Node affinities are learned using an attention-style mecha-

nism:

$$\tilde{e}_{ij} = \text{LeakyReLU}(\mathbf{a}^\top [W_u \mathbf{u}_i \| W_u \mathbf{u}_j]), \quad (19)$$

$$\alpha_{ij} = \frac{\exp(\tilde{e}_{ij})}{\sum_{k=1}^N \exp(\tilde{e}_{ik})} \in \mathbf{A}^{(\text{ag})}. \quad (20)$$

The resulting adjacency is symmetrized and normalized:

$$\mathbf{A}^{(\text{sym})} = \frac{1}{2} (\mathbf{A}^{(\text{ag})} + (\mathbf{A}^{(\text{ag})})^\top), \quad \widehat{\mathbf{A}} = \tilde{\mathbf{D}}^{-\frac{1}{2}} \mathbf{A}^{(\text{sym})} \tilde{\mathbf{D}}^{-\frac{1}{2}}, \quad (21)$$

where $\tilde{\mathbf{D}}$ is the degree matrix of $\mathbf{A}^{(\text{sym})}$. If prior adjacency \mathbf{A}_0 is available, we blend the two sources:

$$\mathbf{A}^* = \lambda \mathbf{A}_0 + (1 - \lambda) \widehat{\mathbf{A}}, \quad \lambda \in [0, 1]. \quad (22)$$

Graph-enhanced Spatial Mixing. Using the learned adjacency \mathbf{A}^* , the block performs graph convolution at each time step:

$$\mathbf{G}_{:,t} = \sigma\left(\mathbf{A}^* (W_g \mathbf{X}_{:,t}^{(s)}) + b_g\right). \quad (23)$$

A residual connection stabilizes learning:

$$\mathbf{G} \leftarrow \mathbf{G} + \mathbf{X}^{(s)}. \quad (24)$$

Temporal and Channel Mixing. Temporal dependencies are modeled via a State-Space Module (SSM), followed by channel mixing:

$$\mathbf{T}_{i,:} = \text{SSM}(\mathbf{G}_{i,:}) + \mathbf{G}_{i,:}, \quad (25)$$

$$\mathbf{C}_{i,t} = \text{MLP}_{\text{chan}}(\text{LayerNorm}(\mathbf{T}_{i,t})) + \mathbf{T}_{i,t}. \quad (26)$$

Projection and Residual Refinement. The block output is produced by projecting back to the original dimension with a residual connection:

$$\mathbf{O} = \text{LayerNorm}(W_o \mathbf{C} + b_o) + \mathbf{X}^{(s)}. \quad (27)$$

Multi-scale Fusion and Skip Connections. During decoding, the upsampled representation at scale s is fused with the encoder’s corresponding feature $\mathbf{Y}^{(s)}$ via concatenation and projection:

$$\mathbf{Z}^{(s)} = \text{Fuse}(\mathbf{Y}^{(s)}, \widehat{\mathbf{Y}}^{(s)}) = \text{Proj}([\mathbf{Y}^{(s)}; \widehat{\mathbf{Y}}^{(s)}]). \quad (28)$$

The fused tensor is passed through another G-Mamba block, enabling joint refinement of encoder and decoder information.

3.3 Uncertainty-aware Prediction

We design a modular uncertainty quantification component atop the GraphMamba backbone that produces calibrated uncertainty estimates. This component comprises three complementary mechanisms, node-based, distribution-based, and parameter-based uncertainty quantification, which together capture local heteroscedasticity, predictive distributional shape, and epistemic uncertainty.

Node-based Uncertainty

Node-based uncertainty produces per-node prediction intervals expressing local uncertainty at the region level. For a prediction target $y_{i,t+\tau}$ at node i and horizon τ , we learn lower and upper quantile heads $\ell_\alpha(i, t, \tau)$ and $u_\alpha(i, t, \tau)$ for a nominal miscoverage level α (e.g., $\alpha = 0.1$ for a 90% interval).

Each quantile head is implemented as a projection from the backbone’s final hierarchical representation \mathbf{Z} . The pinball loss for a set \mathcal{Q} of quantile levels is:

$$\mathcal{L}_{\text{quant}} = \frac{1}{|\mathcal{Q}|} \sum_{q \in \mathcal{Q}} \frac{1}{|\mathcal{S}|} \sum_{(i,t+\tau) \in \mathcal{S}} \rho_q(y_{i,t+\tau} - \hat{q}_{i,t+\tau}), \quad (29)$$

where $\rho_q(z) = \max(qz, (q-1)z)$ is the pinball loss, $\hat{q}_{i,t+\tau}$ denotes the predicted q -quantile, and \mathcal{S} is the training set. Node-based intervals are robust to misspecification of the full predictive distribution, as they directly target coverage without assuming any parametric form.

Distribution-based Uncertainty

Distribution-based uncertainty fits a parametric predictive distribution (e.g., Gaussian or Laplace) per node-time. The most common instantiation is a heteroscedastic Gaussian predictor outputting mean $\mu_{i,t+\tau}$ and variance $\sigma_{i,t+\tau}^2$:

$$p(y_{i,t+\tau} | \mathbf{x}) = \mathcal{N}(y_{i,t+\tau}; \mu_{i,t+\tau}, \sigma_{i,t+\tau}^2). \quad (30)$$

This head is trained by minimizing the negative log likelihood (NLL):

$$\mathcal{L}_{\text{nll}} = \frac{1}{|\mathcal{S}|} \sum_{(i,t+\tau) \in \mathcal{S}} \left(\frac{1}{2} \log \sigma_{i,t+\tau}^2 + \frac{(y_{i,t+\tau} - \mu_{i,t+\tau})^2}{2\sigma_{i,t+\tau}^2} \right). \quad (31)$$

Distribution-based heads capture aleatoric uncertainty (data noise and heteroscedasticity) and allow analytic computation of prediction intervals, e.g., $\mu \pm z_{1-\alpha/2}\sigma$ for Gaussian.

Parameter-based Uncertainty

Parameter-based uncertainty estimates epistemic uncertainty arising from model parameters. We adopt the commonly-used MC Dropout, which performs M stochastic forward passes at inference with dropout enabled. Given M stochastic predictions $\{\mu_{i,t+\tau}^{(m)}\}_{m=1}^M$ and $\{\sigma_{i,t+\tau}^{2,(m)}\}_{m=1}^M$, the predictive mean and total variance decompose as:

$$\widehat{\mu}_{i,t+\tau} = \frac{1}{M} \sum_{m=1}^M \mu_{i,t+\tau}^{(m)}, \quad (32)$$

$$\text{Var}_{\text{pred}}(y) = \underbrace{\frac{1}{M} \sum_{m=1}^M \sigma_{i,t+\tau}^{2,(m)}}_{\text{aleatoric}} + \underbrace{\frac{1}{M} \sum_{m=1}^M (\mu_{i,t+\tau}^{(m)} - \widehat{\mu}_{i,t+\tau})^2}_{\text{epistemic}}. \quad (33)$$

This decomposition yields interval estimates that combine both sources of aleatoric and epistemic uncertainty. The parameter-based loss minimizes the variance of ensemble predictions to encourage consistency, i.e., the model should produce similar predictions across different dropout masks when it is confident about a given input:

$$\mathcal{L}_{\text{param}} = \frac{1}{|\mathcal{S}|} \sum_{(i,t+\tau) \in \mathcal{S}} \frac{1}{M} \sum_{m=1}^M (\mu_{i,t+\tau}^{(m)} - \widehat{\mu}_{i,t+\tau})^2. \quad (34)$$

A lower value of $\mathcal{L}_{\text{param}}$ indicates that the stochastic predictions are tightly clustered around their mean, reflecting lower epistemic uncertainty.

Integrated Training Objective

We jointly train all the above uncertainty heads using:

$$\mathcal{L}_{\text{total}} = \mathcal{L}_{\text{quant}} + \mathcal{L}_{\text{nll}} + \mathcal{L}_{\text{param}} + \mathcal{L}_{\text{calib}}, \quad (35)$$

where $\mathcal{L}_{\text{quant}}$, \mathcal{L}_{nll} , and $\mathcal{L}_{\text{param}}$ correspond to node-based, distribution-based, and parameter-based uncertainty losses, respectively. The calibration loss $\mathcal{L}_{\text{calib}}$ encourages standardized residuals to match a standard normal distribution. Over a training minibatch \mathcal{B} , we compute

$$\mathcal{L}_{\text{calib}} = \left(\frac{1}{|\mathcal{B}|} \sum_{(i, t+\tau) \in \mathcal{B}} r_{i, t+\tau} \right)^2 + \left(\frac{1}{|\mathcal{B}|} \sum_{(i, t+\tau) \in \mathcal{B}} r_{i, t+\tau}^2 - 1 \right)^2, \quad (36)$$

which enforces the standardized residuals to have zero mean and unit variance, thereby improving probabilistic calibration. Here, the standardized residual is defined as

$$r_{i, t+\tau} = \frac{y_{i, t+\tau} - \mu_{i, t+\tau}}{\sigma_{i, t+\tau} + \varepsilon}, \quad (37)$$

where $\varepsilon > 0$ is a small constant for numerical stability.

Post-hoc Quantile Calibration

To improve the empirical coverage of the trained quantile intervals, we apply a post-hoc quantile calibration on a held-out calibration set. Let (ℓ_i, u_i) be the predicted interval and y_i be the ground truth, we compute the empirical coverage gap:

$$\Delta_{\text{cov}} = (1 - \alpha) - \frac{1}{|\mathcal{C}|} \sum_{i \in \mathcal{C}} \mathbf{1}[\ell_i \leq y_i \leq u_i], \quad (38)$$

where \mathcal{C} is the calibration set and α is the target miscoverage level. We then compute the adjustment margin:

$$c = \text{Quantile}_{1-\alpha} \left\{ \max\{\ell_i - y_i, y_i - u_i, 0\} \right\}_{i \in \mathcal{C}}. \quad (39)$$

The calibrated interval for a new prediction becomes

$$[\ell^{\text{cal}}, u^{\text{cal}}] = [\ell - c, u + c], \quad (40)$$

which adjusts the quantile regression intervals to achieve the target coverage level.

4 Evaluation

In this section, we conduct a comprehensive experimental evaluation of our proposed HealthMamba. Specifically, we aim to address the following five research questions:

- **RQ 1:** How does HealthMamba perform compared to state-of-the-art baselines?
- **RQ 2:** Is HealthMamba effective for visit prediction of different types of healthcare facilities?
- **RQ 3:** Are all components in HealthMamba effective?
- **RQ 4:** How does HealthMamba perform under abnormal scenarios such as public emergencies (COVID-19)?
- **RQ 5:** Is HealthMamba computationally efficient?

4.1 Evaluation Setup

Datasets. We utilize healthcare facility visit data from four major U.S. states (California, New York, Texas, and Florida), provided by SafeGraph. The dataset captures daily visit counts to four categories (i.e., Ambulatory Health Care Services, Hospitals, Nursing and Residential Care Facilities, and Social Assistance) of healthcare facilities at the county level from January 2019 to April 2022, spanning 40 months.

Baselines. We compare HealthMamba with 5 categories of 13 state-of-the-art baselines: (1) GNN-based: DCRNN [Li *et al.*, 2017], STGCN [Yu *et al.*, 2018], AGCRN [Bai *et al.*, 2020], DGCRN [Li *et al.*, 2023], UQGNN [Yu *et al.*, 2025]; (2) Attention-based: DSTAGNN [Lan *et al.*, 2022], ASTGCN [Zhu *et al.*, 2021]; (3) Transformer-based: GluonTS [Alexandrov *et al.*, 2020], PatchTST [Nie, 2022]; (4) LLM-based: ST-LLM [Liu *et al.*, 2024], UrbanGPT [Li *et al.*, 2024]; (5) Mamba-based: Mamba [Gu and Dao, 2024], U-Mamba [Ma *et al.*, 2024]. Detailed descriptions and parameter settings of baselines are in Appendix C.1.

Metrics. We utilize two widely used metrics, including Mean Absolute Error (MAE) and Root Mean Squared Error (RMSE), to evaluate the performance of deterministic prediction, and three other commonly used metrics, including Mean Prediction Interval Width (MPIW), Interval Score (IS), and Coverage (COV), to evaluate the performance of uncertainty quantification. Details are in Appendix C.2. It is worth noting that our model outputs prediction intervals, and the deterministic metrics are computed based on the mean of the upper and lower bounds.

4.2 Overall Performance Comparison (RQ 1)

An overall comparison of our HealthMamba and other baselines is presented in Table 1. We found that our HealthMamba reduces MAE by approximately 6.0% compared to the best baseline Mamba based on the average of all four datasets. In addition, HealthMamba also demonstrates superior performance on prediction reliability, with a 3.5% improvement in IS and reaching the target coverage. As shown in Figure 2, the green shadow of HealthMamba is more compact while still covering most observations, indicating more reliable and precise estimates compared to baselines. Our experiments show that HealthMamba consistently achieves the best performance for both short-term (next-day) and medium-term (7-day-ahead) prediction, and the details are in Appendix D.

4.3 Type-specific Visit Prediction (RQ 2)

We further show the prediction results on different healthcare facility categories in Table 2. We found that HealthMamba consistently outperforms Mamba and UrbanGPT across all categories. Notably, Mamba fails to achieve target coverage in the Nursing and Social categories, while UrbanGPT exhibits substantially wider prediction intervals despite achieving coverage. In contrast, HealthMamba maintains valid and compact confidence intervals across all categories, demonstrating robustness to facility-type heterogeneity.

4.4 Ablation Study (RQ 3)

To evaluate the contribution of each key component in HealthMamba, we conduct an ablation study by comparing

Table 1: Comparison with state-of-the-art baselines on four datasets with a horizon of 3 days. \downarrow indicates lower is better. The best results are in **bold** and the second-best are underlined. \checkmark indicates target coverage ($\geq 90\%$) achieved, while \times indicates failure.

		California					New York				
Category	Method	MAE \downarrow	RMSE \downarrow	MPIW \downarrow	IS \downarrow	COV	MAE \downarrow	RMSE \downarrow	MPIW \downarrow	IS \downarrow	COV
GNN	DCRNN	30.537	98.941	76.215	229.083	\times	10.957	35.371	55.028	65.715	\checkmark
	STGCN	32.708	95.427	120.883	203.678	\times	8.967	34.218	36.705	55.320	\times
	AGCRN	17.494	56.480	46.071	130.347	\times	6.453	21.913	17.106	47.504	\times
	DGCRN	28.408	84.729	96.559	208.084	\times	17.526	57.587	19.001	273.164	\times
	UQGNN	10.235	36.520	35.680	77.672	\checkmark	4.585	15.820	15.230	30.426	\checkmark
Attention	DSTAGNN	20.675	55.261	63.458	131.816	\times	8.234	29.719	32.791	49.481	\times
	ASTGCN	47.249	178.047	50.549	749.407	\times	16.679	60.544	15.101	267.103	\times
Transformer	GluonTS	16.945	44.336	87.273	107.044	\times	4.900	16.220	26.784	33.798	\checkmark
	PatchTST	12.381	36.301	59.704	80.008	\times	5.555	20.426	29.517	37.260	\checkmark
LLM	ST-LLM	14.391	47.347	37.231	111.233	\times	5.565	20.800	16.181	38.178	\times
	UrbanGPT	9.734	38.925	47.906	83.962	\checkmark	4.870	17.685	20.866	31.100	\checkmark
Mamba	Mamba	9.467	35.825	33.306	77.232	\checkmark	4.176	14.152	14.174	30.608	\times
	U-Mamba	10.052	34.180	37.561	78.868	\times	4.292	14.993	16.798	29.958	\times
Ours	HealthMamba	9.150	33.401	30.970	74.953	\checkmark	3.926	<u>14.395</u>	14.110	29.361	\checkmark
Texas											
Category	Method	MAE \downarrow	RMSE \downarrow	MPIW \downarrow	IS \downarrow	COV	MAE \downarrow	RMSE \downarrow	MPIW \downarrow	IS \downarrow	COV
GNN	DCRNN	25.612	178.462	34.506	344.785	\times	185.410	418.957	403.593	856.315	\times
	STGCN	22.176	164.037	75.763	165.212	\times	168.203	385.663	489.048	786.315	\times
	AGCRN	8.632	54.573	21.883	93.392	\times	114.045	277.833	468.500	643.579	\times
	DGCRN	32.224	201.640	55.081	547.595	\checkmark	175.580	405.767	436.702	927.128	\times
	UQGNN	7.125	49.350	23.580	60.850	\checkmark	72.350	175.620	259.559	465.230	\checkmark
Attention	DSTAGNN	13.805	91.072	49.969	95.638	\times	150.137	355.974	447.363	654.617	\times
	ASTGCN	31.285	197.239	36.954	580.777	\times	170.262	418.748	357.474	871.215	\times
Transformer	GluonTS	7.502	50.466	37.472	61.071	\checkmark	120.852	282.507	539.905	700.880	\times
	PatchTST	28.904	191.871	25.174	450.373	\times	167.780	370.929	253.671	845.201	\times
LLM	ST-LLM	8.921	60.350	17.686	87.761	\checkmark	99.501	224.992	340.592	616.386	\times
	UrbanGPT	11.024	67.689	48.997	66.529	\checkmark	<u>58.459</u>	<u>158.116</u>	307.648	<u>436.149</u>	\checkmark
Mamba	Mamba	6.676	47.318	24.595	61.466	\times	85.793	209.168	386.492	567.448	\times
	U-Mamba	7.283	50.011	23.887	60.232	\times	85.256	221.271	315.136	624.394	\times
Ours	HealthMamba	6.275	46.566	24.015	58.934	\checkmark	54.951	156.535	<u>255.230</u>	420.884	\checkmark

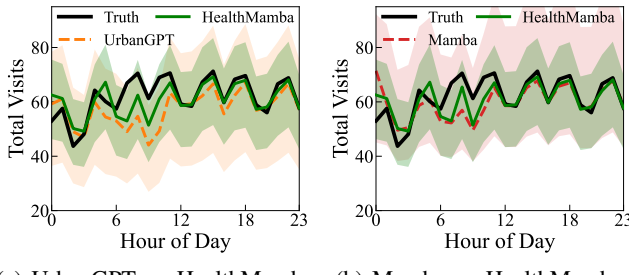


Figure 2: Prediction results on the California dataset aggregated in 24 hours, with best baselines selected for visualization.

the full model against six variants: (1) **w/o STCE**, which removes the contextual information; (2) **w/o G-Mamba**, which

Table 2: Fine-grained prediction on four healthcare facility types.

Category	Model	MAE \downarrow	RMSE \downarrow	MPIW \downarrow	IS \downarrow	COV
Hospitals	Mamba	12.384	42.156	38.720	95.832	\checkmark
	UrbanGPT	12.058	45.623	52.418	101.254	\checkmark
	HealthMamba	11.628	39.524	35.105	91.250	\checkmark
Ambulatory	Mamba	8.152	31.478	29.640	68.425	\checkmark
	UrbanGPT	8.536	34.127	42.815	73.680	\checkmark
	HealthMamba	7.683	29.352	27.218	65.127	\checkmark
Nursing	Mamba	7.945	28.634	31.852	62.148	\times
	UrbanGPT	8.213	32.576	45.037	70.425	\checkmark
	HealthMamba	7.486	26.815	29.476	59.268	\checkmark
Social	Mamba	9.387	40.032	33.012	82.523	\times
	UrbanGPT	10.127	43.374	51.352	89.489	\checkmark
	HealthMamba	8.803	37.913	31.081	78.167	\checkmark

Table 3: Ablation study on the California dataset.

Variants	MAE↓	RMSE↓	MPIW↓	IS↓	COV
w/o STCE	13.610	48.535	39.807	108.110	✗
w/o G-Mamba	15.782	49.092	42.625	117.382	✗
w/o Node-based	9.682	34.925	32.540	80.115	✗
w/o Distribution-based	10.154	36.218	34.112	85.330	✗
w/o Parameter-based	10.573	37.665	35.890	90.224	✗
w/o UQ (Total)	11.240	39.150	37.520	-	-
HealthMamba	9.150	33.401	30.970	74.953	✓

replaces the GraphMamba with conventional Mamba; (3) **w/o Node-based** UQ module, (4) **w/o Distribution-based** UQ module, and (5) **w/o Parameter-based** UQ module; and (6) **w/o UQ**, which uses only quantile regression.

From Table 3, we verify the effectiveness of our design from multiple perspectives. First, regarding the general architecture, the performance without GraphMamba suffers the most significant degradation (MAE increases to 15.782), highlighting the importance of capturing spatiotemporal dependencies. Similarly, removing STCE leads to a substantial increase in error, verifying the necessity of integrating contextual information. Second, we observe that removing the Node-based, Parameter-based, or Distribution-based UQ modules individually leads to suboptimal performance (MAE ranges from 9.682 to 10.573). Crucially, without the synergy of these components, the model fails to satisfy the coverage constraint, i.e., COV becomes ✗. Finally, while the w/o UQ variant achieves a relatively lower MAE compared to other incomplete variants, it cannot completely provide valid intervals, as shown by missing values for IS and COV metrics.

4.5 Prediction under Abnormal Situations (RQ 4)

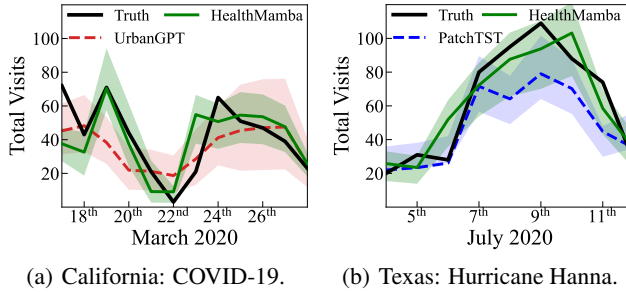


Figure 3: Prediction results under extreme events.

A key challenge in healthcare facility visit prediction is handling abnormal scenarios, such as public emergencies and extreme weather events, which usually cause sudden deviations in visit patterns. Accurate and reliable prediction under these abnormal scenarios is critical for emergency preparedness and resource allocation. We utilize two representative events to show the effectiveness of our method: (1) the COVID-19 pandemic lockdown in Los Angeles County, California (March 2020), where the statewide stay-at-home order

caused a sudden drop in healthcare facility visits, and (2) Hurricane Hanna in Texas (July 2020), which caused a sudden surge in emergency healthcare facility visits. As shown in Figure 3, under these situations, HealthMamba successfully maintained accurate predictions, and ground truth values are also within the prediction intervals in most cases, whereas the best baseline struggled to adapt to these abrupt changes. These results highlight HealthMamba’s superior adaptability to both demand surges and drops under abnormal scenarios.

4.6 Complexity Analysis (RQ 5)

We study the computational complexity of HealthMamba in terms of training time per epoch, peak GPU memory usage, and the number of parameters. We found HealthMamba achieves a good balance between model capacity and computational efficiency, with 65 seconds for training time per epoch, 1.5 GB memory, and 892K parameters, which is comparable to the best baselines and more efficient than LLM-based methods. More details are provided in Appendix D.

5 Related Work

5.1 Healthcare Facility Visit Prediction

Healthcare facility visit prediction has attracted much interest from both academia and the government, as it is important for health resource allocation and public emergency responses. Traditional methods rely on statistical models such as ARIMA [Alghamdi *et al.*, 2019; Orhan and Kuruksen, 2025] and regression-based methods [Pun *et al.*, 2019; Avinash *et al.*, 2025] for daily or weekly patient count prediction, but overlook temporal dynamics and spatial dependencies. Recent works have explored different approaches to address this problem, including GNN-based methods [Yu *et al.*, 2018], attention-based methods [Lan *et al.*, 2022], Transformer-based methods [Nie, 2022], and LLM-based methods [Li *et al.*, 2024]. However, most existing works focus on aggregated prediction without considering different types of healthcare facilities, such as hospitals, ambulatory health care services, and nursing facilities, which is more important for practical decision support. In addition, existing solutions usually consider this problem a time-series prediction problem, without capturing spatial dependencies, which can potentially be used to improve prediction performance.

5.2 Uncertainty-aware Spatiotemporal Prediction

Uncertainty quantification has attracted much interest from the spatiotemporal prediction community because it lays the foundation for reliable and safe decision-making [Wen *et al.*, 2023; Zhuang *et al.*, 2022]. DeepSTUQ [Qian *et al.*, 2023] employs dual sub-networks to separately quantify aleatoric and epistemic uncertainty at each node. DiffSTG [Wen *et al.*, 2023] generalizes denoising diffusion probabilistic models to spatiotemporal graphs to capture intrinsic uncertainties. STZINB-GNN [Zhuang *et al.*, 2022] models sparse spatiotemporal data through zero-inflated negative binomial distributions. CF-GNN [Huang *et al.*, 2024] extends conformal prediction to graph-based models for guaranteed coverage, providing distribution-free prediction intervals. UQGNN [Yu

et al., 2025] integrates graph neural networks with node-level uncertainty estimation for spatiotemporal prediction.

Different from existing works, in this paper, we design a comprehensive uncertainty quantification module that integrates distribution-based, parameter-based, and node-based uncertainty quantification mechanisms, combined with post-hoc quantile calibration to produce well-calibrated prediction intervals for uncertainty-aware spatiotemporal prediction.

6 Conclusion

In this paper, we propose HealthMamba, an uncertainty-aware spatiotemporal framework for accurate and reliable healthcare facility visit prediction. There are three key components in HealthMamba: (i) a Unified Spatiotemporal Context Encoder that integrates both heterogeneous static and dynamic contextual information, (ii) a novel graph state space model called GraphMamba for spatiotemporal modeling, and (iii) a comprehensive UQ module integrating three different types of UQ mechanisms and a post-hoc quantile calibration for higher prediction reliability. Extensive experiments on four real-world datasets from California, New York, Texas, and Florida demonstrate that HealthMamba outperforms 13 state-of-the-art baselines, improving prediction accuracy by 6.0% and uncertainty quantification by 3.5%. Our uncertainty-aware design also enables robust predictions under public emergencies and extreme weather events, supporting trustworthy decision-making under abnormal scenarios.

Ethics Statement

All authors have read and agree to abide by the IJCAI Code of Ethics. This research uses only de-identified datasets and does not involve human subjects, personally identifiable information, or sensitive private data. The study poses no foreseeable risk of harm to individuals or groups, and all experiments were conducted in compliance with applicable laws and institutional policies. No conflicts of interest or external sponsorship that could bias the results are present. We take full responsibility for the integrity of the data, the analyses, and the conclusions presented in this paper.

References

[Alexandrov *et al.*, 2020] Alexander Alexandrov, Konstantinos Benidis, Michael Bohlke-Schneider, Valentin Flunkert, Jan Gasthaus, Tim Januschowski, Danielle C Maddix, Syama Rangapuram, David Salinas, Jasper Schulz, et al. Gluonts: Probabilistic and neural time series modeling in python. *Journal of Machine Learning Research*, 21(116):1–6, 2020.

[Alghamdi *et al.*, 2019] Taghreed Alghamdi, Khalid Elgazar, Magdi Bayoumi, Taysseer Sharaf, and Sumit Shah. Forecasting traffic congestion using arima modeling. In *2019 15th International Wireless Communications & Mobile Computing Conference (IWCMC)*, pages 1227–1232, 2019.

[Avinash *et al.*, 2025] G Avinash, Hariom Pachori, Avinash Sharma, and SukhDev Mishra. Time series forecasting of bed occupancy in mental health facilities in india using machine learning. *Scientific Reports*, 15(1):2686, 2025.

[Bai *et al.*, 2020] Lei Bai, Lina Yao, Can Li, Xianzhi Wang, and Can Wang. Adaptive graph convolutional recurrent network for traffic forecasting. *Advances in neural information processing systems*, 33:17804–17815, 2020.

[Brossard *et al.*, 2025] Cyrielle Brossard, Christophe Goetz, Pierre Catoire, Lauriane Cipolat, Christophe Guyeux, Cédric Gil Jardine, Mahuna Akplogan, and Laure Abensur Vuillaume. Predicting emergency department admissions using a machine-learning algorithm: a proof of concept with retrospective study. *BMC Emergency Medicine*, 25(1):3, 2025.

[Gu and Dao, 2024] Albert Gu and Tri Dao. Mamba: Linear-time sequence modeling with selective state spaces. In *First conference on language modeling*, 2024.

[Guo *et al.*, 2021] Shengnan Guo, Youfang Lin, Huaiyu Wan, Xiucheng Li, and Gao Cong. Learning dynamics and heterogeneity of spatial-temporal graph data for traffic forecasting. *IEEE Transactions on Knowledge and Data Engineering*, 34(11):5415–5428, 2021.

[Huang *et al.*, 2024] Kexin Huang, Ying Jin, Emmanuel Candes, and Jure Leskovec. Uncertainty quantification over graph with conformalized graph neural networks. *Advances in Neural Information Processing Systems*, 36, 2024.

[Karsanti *et al.*, 2019] Hayuning Titi Karsanti, Igi Ardiyanto, and Lukito Edi Nugroho. Deep learning-based patient visits forecasting using long short term memory. In *2019 international conference of artificial intelligence and information technology (icait)*, pages 344–349. IEEE, 2019.

[Lan *et al.*, 2022] Shiyong Lan, Yitong Ma, Weikang Huang, Wenwu Wang, Hongyu Yang, and Pyang Li. Dstagnn: Dynamic spatial-temporal aware graph neural network for traffic flow forecasting. In *International conference on machine learning*, pages 11906–11917. PMLR, 2022.

[Li *et al.*, 2017] Yaguang Li, Rose Yu, Cyrus Shahabi, and Yan Liu. Diffusion convolutional recurrent neural network: Data-driven traffic forecasting. *arXiv preprint arXiv:1707.01926*, 2017.

[Li *et al.*, 2022] Weiyu Li, Qi Wang, Yuanyuan Liu, Mario L Small, and Jianxi Gao. A spatiotemporal decay model of human mobility when facing large-scale crises. *Proceedings of the National Academy of Sciences*, 119(33):e2203042119, 2022.

[Li *et al.*, 2023] Fuxian Li, Jie Feng, Huan Yan, Guangyin Jin, Fan Yang, Funing Sun, Depeng Jin, and Yong Li. Dynamic graph convolutional recurrent network for traffic prediction: Benchmark and solution. *ACM Transactions on Knowledge Discovery from Data*, 17(1):1–21, 2023.

[Li *et al.*, 2024] Zhonghang Li, Lianghao Xia, Jiabin Tang, Yong Xu, Lei Shi, Long Xia, Dawei Yin, and Chao Huang. Urbangpt: Spatio-temporal large language models. In *Proceedings of the 30th ACM SIGKDD Conference on Knowledge Discovery and Data Mining*, pages 5351–5362, 2024.

[Lim *et al.*, 2021] Bryan Lim, Sercan Ö Arik, Nicolas Loeff, and Tomas Pfister. Temporal fusion transformers for interpretable multi-horizon time series forecasting. *International journal of forecasting*, 37(4):1748–1764, 2021.

[Liu *et al.*, 2024] Ruyang Liu, Chen Li, Haoran Tang, Yixiao Ge, Ying Shan, and Ge Li. St-llm: Large language models are effective temporal learners. In *European Conference on Computer Vision*, pages 1–18. Springer, 2024.

[Ma *et al.*, 2024] Jun Ma, Feifei Li, and Bo Wang. U-mamba: Enhancing long-range dependency for biomedical image segmentation. *arXiv preprint arXiv:2401.04722*, 2024.

[Marcusson *et al.*, 2020] Jan Marcusson, Magnus Nord, Huan-Ji Dong, and Johan Lyth. Clinically useful prediction of hospital admissions in an older population. *BMC geriatrics*, 20(1):95, 2020.

[Nie, 2022] Y Nie. A time series is worth 64words: Long-term forecasting with transformers. *arXiv preprint arXiv:2211.14730*, 2022.

[Orhan and Kurutkan, 2025] Fatih Orhan and Mehmet Nuruallah Kurutkan. Predicting total healthcare demand using machine learning: separate and combined analysis of predisposing, enabling, and need factors. *BMC Health Services Research*, 25(1):366, 2025.

[Piccialli *et al.*, 2020] Francesco Piccialli, Salvatore Cuomo, Danilo Crisci, Edoardo Prezioso, and Gang Mei. A deep learning approach for facility patient attendance prediction based on medical booking data. *Scientific Reports*, 10(1):14623, 2020.

[Pun *et al.*, 2019] Lilian Pun, Pengxiang Zhao, and Xintao Liu. A multiple regression approach for traffic flow estimation. *IEEE Access*, 7:35998–36009, 2019.

[Qian *et al.*, 2023] Weizhu Qian, Dalin Zhang, Yan Zhao, Kai Zheng, and James JQ Yu. Uncertainty quantification for traffic forecasting: A unified approach. In *2023 IEEE 39th International Conference on Data Engineering (ICDE)*, pages 992–1004. IEEE, 2023.

[Salinas *et al.*, 2020] David Salinas, Valentin Flunkert, Jan Gasthaus, and Tim Januschowski. Deepar: Probabilistic forecasting with autoregressive recurrent networks. *International journal of forecasting*, 36(3):1181–1191, 2020.

[Shah *et al.*, 2022] Abhin Shah, Yuheng Bu, Joshua K Lee, Subhro Das, Rameswar Panda, Prasanna Sattigeri, and Gregory W Wornell. Selective regression under fairness criteria. In *International Conference on Machine Learning*, pages 19598–19615. PMLR, 2022.

[Skianis *et al.*, 2023] Konstantinos Skianis, Giannis Nikoletzos, Benoit Gallix, Rodolphe Thiebaut, and Georgios Exarchakis. Predicting covid-19 positivity and hospitalization with multi-scale graph neural networks. *Scientific Reports*, 13(1):5235, 2023.

[Sokol *et al.*, 2024] Anna Sokol, Nuno Moniz, and Nitesh Chawla. Conformalized selective regression. *arXiv preprint arXiv:2402.16300*, 2024.

[Tang *et al.*, 2023] Siyi Tang, Amara Tariq, Jared A Dunnmon, Umesh Sharma, Praneetha Elugunti, Daniel L Rubin, Bhavik N Patel, and Imon Banerjee. Predicting 30-day all-cause hospital readmission using multimodal spatiotemporal graph neural networks. *IEEE Journal of Biomedical and Health Informatics*, 27(4):2071–2082, 2023.

[Tuominen *et al.*, 2024] Jalmari Tuominen, Eetu Pulkkinen, Jaakko Peltonen, Juho Kanniainen, Niku Oksala, Ari Palomäki, and Antti Roine. Forecasting emergency department occupancy with advanced machine learning models and multivariable input. *International Journal of Forecasting*, 40(4):1410–1420, 2024.

[Wen *et al.*, 2023] Haomin Wen, Youfang Lin, Yutong Xia, Huaiyu Wan, Qingsong Wen, Roger Zimmermann, and Yuxuan Liang. Diffstg: Probabilistic spatio-temporal graph forecasting with denoising diffusion models. In *Proceedings of the 31st ACM International Conference on Advances in Geographic Information Systems*, pages 1–12, 2023.

[Xu *et al.*, 2023] Ran Xu, Xiao Huang, Kai Zhang, Weixuan Lyu, Debarchana Ghosh, Zhenlong Li, and Xiang Chen. Integrating human activity into food environments can better predict cardiometabolic diseases in the united states. *Nature communications*, 14(1):7326, 2023.

[Yu *et al.*, 2018] Bing Yu, Haoteng Yin, and Zhanxing Zhu. Spatio-temporal graph convolutional networks: a deep learning framework for traffic forecasting. *Proceedings of the 27th International Joint Conference on Artificial Intelligence*, page 3634–3640, 2018.

[Yu *et al.*, 2025] Dahai Yu, Dingyi Zhuang, Lin Jiang, Rongchao Xu, Xinyue Ye, Yuheng Bu, Shenhao Wang, and Guang Wang. Uqgnn: Uncertainty quantification of graph neural networks for multivariate spatiotemporal prediction. In *Proceedings of the 33rd ACM International Conference on Advances in Geographic Information Systems*, pages 52–65, 2025.

[Zhang *et al.*, 2022] Yan Zhang, Jie Zhang, Min Tao, Jian Shu, and Degang Zhu. Forecasting patient arrivals at emergency department using calendar and meteorological information. *Applied Intelligence*, 52(10):11232–11243, 2022.

[Zhong *et al.*, 2026] Yibo Zhong, Haoxiang Jiang, Lincan Li, Ryumei Nakada, Tiansi Liu, Linjun Zhang, Huaxiu Yao, and Haoyu Wang. Peanut: Parameter-efficient adaptation with weight-aware neural tweakers. In *Proceedings of the 32nd ACM SIGKDD Conference on Knowledge Discovery and Data Mining*, 2026.

[Zhu *et al.*, 2021] Jiawei Zhu, Qiongjie Wang, Chao Tao, Hanhan Deng, Ling Zhao, and Haifeng Li. Ast-gen: Attribute-augmented spatiotemporal graph convolutional network for traffic forecasting. *IEEE Access*, 9:35973–35983, 2021.

[Zhuang *et al.*, 2022] Dingyi Zhuang, Shenhao Wang, Haris Koutsopoulos, and Jinhua Zhao. Uncertainty quantification of sparse travel demand prediction with spatial-temporal graph neural networks. In *Proceedings of the 28th ACM SIGKDD Conference on Knowledge Discovery and Data Mining*, KDD ’22, page 4639–4647, New York, NY, USA, 2022. Association for Computing Machinery.

Appendix

A Data Analysis

The healthcare facilities are categorized into the following four distinct types by the North American Industry Classification System (NAICS):

- **Code 621: Ambulatory Health Care Services.** Outpatient services without overnight stays, including physicians' and dentists' offices, outpatient surgical centers, urgent care clinics, and home-health agencies. These facilities primarily deliver medical treatment, diagnosis, and minor procedures on an ambulatory basis.
- **Code 622: Hospitals.** Institutions offering comprehensive inpatient medical, surgical, and diagnostic services. This type includes both general hospitals and specialized facilities like psychiatric and rehabilitation hospitals.
- **Code 623: Nursing and Residential Care Facilities.** Long-term care institutions providing residential and nursing services for individuals requiring daily living assistance or continuous medical supervision, e.g., nursing homes, skilled-nursing facilities, assisted-living centers, and group homes for persons with disabilities.
- **Code 624: Social Assistance.** Non-residential establishments that offer community-based support and welfare services, including child and family service agencies, rehabilitation and counseling centers, and other organizations promoting social and public well-being.

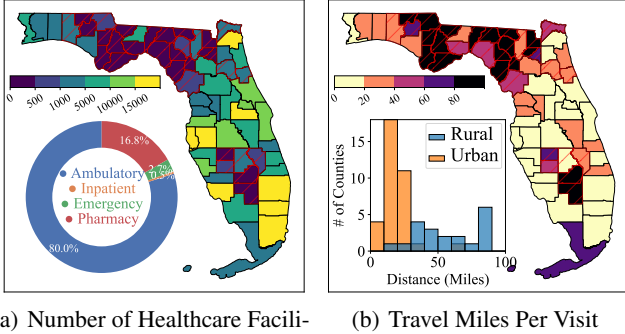


Figure 4: Statistics of the Florida dataset. Red diagonal lines indicate rural counties.

Based on our analysis of the Florida dataset, we have the following findings.

(1) **Uneven Facility Distribution.** Our analysis reveals substantial spatial imbalance in healthcare facility distribution as shown in Figure 4(a). *Ambulatory Care* dominates in terms of facility count, comprising over 60% of all healthcare facilities, with dense clustering in metropolitan areas. *Hospitals* are sparsely distributed, with rural counties often sharing a single hospital or relying on neighboring regions.

(2) **Accessibility Disparities.** Accessibility varies markedly across regions. As depicted in Figure 4(b), rural residents need to travel substantially longer distances, facing

greater barriers to timely care. Visits to *Ambulatory Care* involve the shortest average travel distances (typically under 40 miles), reflecting their widespread availability.

(3) **Heterogeneous Visit Patterns.** Visit behaviors differ considerably across spatial and demographic dimensions. Visit frequency correlates with urbanization level, population aging, and per-capita facility availability. *Nursing Facilities* display stable temporal patterns with gradual long-term trends reflecting demographic shifts, while *Social Assistance* facilities show pronounced monthly patterns, often peaking around benefit distribution dates.

B Pseudocodes

Algorithm 1 STCE: Produce embedding \mathbf{R} from inputs

```

1: Input:  $\mathbf{V} \in \mathbb{R}^{N \times T_{in} \times C}$ ,  $\mathbf{D} \in \mathbb{R}^{N \times d_{dem}}$ ,  $\mathbf{E} \in \mathbb{R}^{N \times T_{in} \times d_{ext}}$ ,  

    $\mathbf{A} \in \mathbb{R}^{N \times N}$ 
2: for each node  $i$  and time  $t$  do
3:    $\mathbf{H}_{i,t}^v, \mathbf{H}_i^d, \mathbf{H}_{i,t}^e \leftarrow \text{FeatureEmbeddingLayers}(\mathbf{v}_{i,t}, \mathbf{D}_i, \mathbf{E}_{i,t})$ 
4:    $\mathbf{X}_{i,t} \leftarrow \mathbf{H}_{i,t}^v + \mathbf{H}_i^d + \mathbf{H}_{i,t}^e$ 
5: end for
6: for each time  $t$  do
7:    $\tilde{\mathbf{X}}_{:,t} \leftarrow \text{GConv}(\mathbf{X}_{:,t}; \mathbf{A})$ 
8: end for
9:  $\tilde{\mathbf{X}} \leftarrow \text{TemporalMixer}(\tilde{\mathbf{X}})$ 
10:  $\mathbf{R} \leftarrow \text{LayerNorm}(\text{Proj}([\tilde{\mathbf{X}}; \mathbf{H}^d]))$ 
11: return  $\mathbf{R} \in \mathbb{R}^{N \times T_{in} \times d_{model}}$ 

```

Algorithm 2 GraphMamba Backbone Forward Pass

```

1: Input:  $\mathbf{X}^{(0)} = \mathbf{R}$ , prior adjacency  $\mathbf{A}_0$ 
2: /* Encoder */
3: for  $s = 0$  to  $S - 1$  do
4:    $\mathbf{Y}^{(s)} \leftarrow \text{G-Mamba}^{(s)}(\mathbf{X}^{(s)}; \mathbf{A}^*)$ 
5:    $\mathbf{X}^{(s+1)} \leftarrow \text{DownConv}(\mathbf{Y}^{(s)})$ 
6: end for
7: /* Bottleneck */
8:  $\mathbf{Y}^{(S)} \leftarrow \text{G-Mamba}^{(S)}(\mathbf{X}^{(S)}; \mathbf{A}^*)$ 
9:  $\mathbf{Z}^{(S)} \leftarrow \mathbf{Y}^{(S)}$ 
10: /* Decoder */
11: for  $s = S - 1$  down to 0 do
12:    $\widehat{\mathbf{Y}}^{(s)} \leftarrow \text{UpConv}(\mathbf{Z}^{(s+1)})$ 
13:    $\mathbf{Z}^{(s)} \leftarrow \text{G-Mamba}^{(s)}(\text{Fuse}(\mathbf{Y}^{(s)}, \widehat{\mathbf{Y}}^{(s)}); \mathbf{A}^*)$ 
14: end for
15: Output: Multi-scale representations  $\{\mathbf{Z}^{(s)}\}_{s=0}^S$ 

```

C Experiment Setup

C.1 Details and Parameters of Baselines

GNN-based Methods

- **DCRNN** [Li *et al.*, 2017]: Diffusion Convolutional Recurrent Neural Network integrates diffusion convolution with a sequence-to-sequence architecture to learn representations

of spatial dependencies and temporal relations. We set the diffusion step to 2 and use a 2-layer seq2seq GRU with hidden size 64; scheduled sampling is enabled and the dropout rate is set to 0.3.

- **STGCN** [Yu *et al.*, 2018]: Spatial-Temporal Graph Convolution Network combines spectral graph convolution with 1D convolution to capture spatial and temporal correlations. The spatial and temporal kernel size is set to 3, the block number is set to 2, and the dropout rate is set to 0.5.
- **AGCRN** [Bai *et al.*, 2020]: An Adaptive Graph Convolutional Recurrent Network that uses a Node Adaptive Parameter Learning module to capture node-specific patterns and a Data Adaptive Graph Generation module to infer inter-dependencies among different traffic series. The order of Chebyshev polynomials is set to 2, the number of blocks is 2, and the RNN unit dimension is set to 64.
- **DGCNN** [Li *et al.*, 2023]: A Dynamic Graph Convolutional Recurrent Network that employs hyper-networks to dynamically generate graph convolutional filters at each time step, capturing evolving spatial dependencies by combining a learned dynamic graph with a pre-defined static road network. We use 2 DGCNN blocks with hidden size 64, set the Chebyshev polynomial order to 2, and apply dropout with rate 0.3.
- **UQGNN** [Yu *et al.*, 2025]: An Uncertainty Quantification Graph Neural Network for multivariate spatiotemporal prediction that introduces an interaction-aware spatiotemporal embedding module along with a multivariate probabilistic prediction module to estimate both expected mean values and associated uncertainties. We use 2 diffusion steps with hidden size 64, set the number of TCN layers to 2 with kernel size 3, and apply dropout with rate 0.3.

Attention-based Methods

- **DSTAGNN** [Lan *et al.*, 2022]: A Dynamic Spatial-Temporal Aware Graph Neural Network that constructs a data-driven, time-varying graph to replace the static topology, using multi-head attention with multi-scale gated convolutions to capture complex spatial and temporal dependencies in traffic flow. We set the number of attention heads to 4, use 2 stacked DSTAGNN layers with hidden size 64, and set the dropout rate to 0.3.
- **ASTGCN** [Guo *et al.*, 2021]: An Attention-based Spatio-Temporal Graph Convolutional Network that employs spatial-temporal attention within graph convolutions, using separate modules for recent, daily-periodic, and weekly-periodic patterns to effectively model dynamic correlations in traffic data. The order of Chebyshev polynomials is set to 2, the number of blocks is also 2, and the time stride is set to 1.

Transformer-based Methods

- **GluonTS** [Alexandrov *et al.*, 2020]: A toolkit for probabilistic time series forecasting that provides deep learning-based models, reference implementations of state-of-the-art methods, and utilities for efficient experimentation and evaluation. We use its probabilistic forecasting backbone with 2 recurrent layers (hidden size 64) and set the context window length to 168; the dropout rate is set to 0.1.
- **PatchTST** [Nie, 2022]: A Transformer-based model for

multivariate time series forecasting that segments each series into subseries-level patches and processes each channel independently, enabling long-range attention and state-of-the-art long-term forecasting performance. We set the patch length to 6 with stride 2, use 3 Transformer encoder layers with 4 attention heads, and set the model dimension to 64 with dropout 0.1.

LLM-based Methods

- **ST-LLM** [Liu *et al.*, 2024]: A Spatial-Temporal Large Language Model for traffic prediction that treats each location’s time series as a sequence of tokens with learned spatial-temporal embeddings, using a partially frozen attention mechanism to capture global spatio-temporal patterns. We adopt a partially frozen LLM and train lightweight adapters; the spatiotemporal embedding dimension is set to 64, and the context length is set to 512 tokens.
- **UrbanGPT** [Li *et al.*, 2024]: A spatio-temporal LLM framework that integrates a dependency encoder with instruction-tuning, enabling the model to learn complex inter-dependencies across time and space and to generalize to diverse urban prediction tasks, especially under data scarcity. We follow the instruction-tuning setup with a dependency encoder of hidden size 64 and 2 layers; the LLM backbone is kept frozen, and the adapter dropout rate is set to 0.1.

Mamba-based Methods

- **Mamba** [Gu and Dao, 2024]: A selective state space model (SSM) architecture that enables efficient long-sequence modeling with linear-time complexity, serving as a strong alternative to attention for capturing long-range temporal dependencies. We use 4 stacked Mamba blocks with model dimension 64 and set the state expansion factor to 2; dropout is set to 0.1.
- **U-Mamba** [Ma *et al.*, 2024]: A U-shaped Mamba architecture that combines hierarchical encoder-decoder processing with skip connections, allowing multi-scale feature extraction while retaining long-range dependency modeling through Mamba blocks. We use a 2-level encoder-decoder with 2 Mamba blocks per stage, set the base width to 64, and apply dropout with rate 0.1.

C.2 Metrics

Deterministic Metrics

We utilize two commonly used deterministic metrics, including Mean Absolute Error (MAE) and Root Mean Squared Error (RMSE), to evaluate the performance of deterministic predictions:

$$\text{MAE} = \frac{1}{N} \sum_{i=1}^N |y_i - \hat{y}_i|, \quad (41)$$

$$\text{RMSE} = \sqrt{\frac{1}{N} \sum_{i=1}^N (y_i - \hat{y}_i)^2}, \quad (42)$$

where y_i is the ground truth label, \hat{y}_i denotes the prediction result, and N is the number of predictions.

Probabilistic Metrics

We also utilize three other metrics, including Mean Prediction Interval Width (MPIW), Interval Score (IS), and Coverage, to evaluate the performance of uncertainty quantification.

MPIW quantifies the average width of prediction intervals a model generates to capture uncertainty in its predictions. Formally, MPIW is defined as:

$$\text{MPIW} = \frac{1}{N} \sum_{i=1}^N (u_{\alpha,i} - l_{\alpha,i}), \quad (43)$$

where $l_{\alpha,i}$ and $u_{\alpha,i}$ are the lower and upper quantile for the i -th prediction under the miscoverage α . Smaller values indicate narrower intervals. MPIW is often used alongside coverage metrics to ensure the prediction intervals balance informativeness and reliability.

It is also important to evaluate the quality of the prediction interval, in addition to calculating the length. Interval Score (IS) evaluates both the width and coverage quality of prediction intervals by penalizing intervals that are too wide or fail to contain the true value. Formally, for miscoverage level α , IS is defined as:

$$\text{IS} = \frac{1}{N} \sum_{i=1}^N \left[(u_{\alpha,i} - l_{\alpha,i}) + \frac{2}{\alpha} (l_{\alpha,i} - y_i) \mathbb{I}(y_i < l_{\alpha,i}) + \frac{2}{\alpha} (y_i - u_{\alpha,i}) \mathbb{I}(y_i > u_{\alpha,i}) \right], \quad (44)$$

where $l_{\alpha,i}$ and $u_{\alpha,i}$ denote the lower and upper bounds of the prediction interval. A smaller values indicate narrower intervals, reflecting higher model confidence.

In addition, we also need to know how the prediction interval covers the ground truth. Given N samples, the prediction interval is denoted as $[l_i, u_i], i = 1, 2, \dots, N$ and the ground truth is expressed as $y_i, i = 1, 2, \dots, N$. The coverage is calculated according to:

$$\text{coverage} = \frac{100\%}{N} \sum_{i=1}^N \mathbb{I}(l_i < y_i < u_i). \quad (45)$$

C.3 Implementation Details

All experiments were conducted on a Linux platform equipped with an NVIDIA A100 GPU with 80 GB of memory. For training, we use the Adam optimizer with a batch size of 128. The initial learning rate is set to 1×10^{-3} , with a decay rate of 5×10^{-4} , applied every 15 epochs. We employ early stopping with a patience of 50 steps based on the validation loss to prevent overfitting. The dataset is divided into training, validation, and testing sets in a ratio of 8:1:1. The input sequence length is set to 7 time steps (7 days), and the model’s output horizon is 3. All time series data are normalized using a transformation of natural logarithm, which is represented as:

$$X' = \ln(X + 1), \quad (46)$$

where X denotes the original dataset and X' is the normalized dataset. All values are incremented by 1 to avoid undefined logarithms for zero-valued entries.

For our proposed HealthMamba, the model dimension d_{model} is set to 64, and the hidden dimension d_{hid} is set to

Table 4: Computational complexity comparison on the California dataset. Train denotes total training time (seconds). Mem denotes peak GPU memory usage (MB). Params denotes the number of trainable parameters (K).

Category	Method	Train↓	Mem↓	Params↓
GNN	DCRNN	83	1,494	25
	STGCN	31	1,621	55
	AGCRN	135	1,567	757
	DGCRN	128	1,539	251
Attention	UQGNN	95	1,580	186
	DSTAGNN	720	1,709	110
Transformer	ASTGCN	72	1,679	66
	GluonTS	70	1,660	28
LLM	PatchTST	35	1,470	77
	ST-LLM	1522	4,280	124,439
Mamba	UrbanGPT	2063	14,336	6,738,415
	Mamba	42	1,700	664
Ours	U-Mamba	58	1,715	804
	HealthMamba	65	1,520	892

128. In the STCE module, the demographic embedding dimension d_{dem} is 32, and the external factor dimension d_{ext} is 16. For the GraphMamba backbone, we use $S = 2$ encoder-decoder stages with 2 Mamba blocks per stage; the state expansion factor is set to 2, and the convolutional kernel size is 4. In the Uncertainty-aware Prediction Head, the target miscoverage rate α is set to 0.1 (corresponding to 90% coverage). Dropout is applied with a rate of 0.3, and gradient clipping is set to 1.0. The ReLU activation function is used before the output to ensure all predictions are non-negative.

D Additional Evaluation

D.1 Detailed Complexity Analysis

We analyze the computational complexity of HealthMamba compared to baselines in terms of training time per epoch, peak GPU memory usage, and the number of parameters. As presented in Table 4, our approach achieves a favorable balance between model capacity and computational efficiency.

In terms of training time, HealthMamba requires 65 seconds per epoch, which is comparable to lightweight models like GluonTS (70s) and ASTGCN (72s), and significantly faster than attention-heavy models like DSTAGNN (720s). Notably, LLM-based methods exhibit substantially higher training costs, with ST-LLM requiring 1,522 seconds and UrbanGPT requiring 2,063 seconds per epoch, approximately 23 \times and 32 \times slower than HealthMamba, respectively.

For GPU memory consumption, HealthMamba uses only 1,520 MB, which is even lower than basic models like STGCN (1,621 MB) and the vanilla Mamba (1,700 MB). This efficient memory footprint is particularly advantageous for deployment scenarios with limited GPU resources. In contrast, LLM-based approaches demand substantially more memory, with UrbanGPT requiring 14,336 MB, nearly 10 \times the memory of HealthMamba.

Regarding parameter count, HealthMamba contains 892K

Table 5: Prediction performance for 1-day prediction horizon. \downarrow indicates lower is better. The best results are in **bold** and the second-best are underlined. ✓ indicates target coverage ($\geq 90\%$) achieved, while ✗ indicates failure.

Category	Method	California					New York				
		MAE \downarrow	RMSE \downarrow	MPIW \downarrow	IS \downarrow	COV	MAE \downarrow	RMSE \downarrow	MPIW \downarrow	IS \downarrow	COV
GNN	DCRNN	23.14	74.89	58.23	172.45	✗	8.23	26.78	41.52	49.33	✗
	STGCN	24.81	72.25	91.88	154.17	✗	6.78	25.91	27.85	41.89	✗
	AGCRN	13.24	42.76	34.89	98.68	✓	4.88	16.59	12.94	35.90	✗
	DGCRN	21.53	64.18	73.29	157.59	✗	13.28	43.64	14.36	206.60	✗
	UQGNN	7.75	27.67	27.03	58.78	✓	3.47	11.98	11.53	22.99	✓
Attention	DSTAGNN	15.67	41.84	48.09	99.82	✓	6.24	22.53	24.89	37.44	✗
	ASTGCN	35.79	134.87	38.32	567.09	✗	12.64	45.84	11.44	202.17	✓
Transformer	GluonTS	12.84	33.58	66.15	81.06	✗	3.71	12.28	20.31	25.60	✗
	PatchTST	9.39	27.50	45.27	60.62	✗	4.21	15.46	22.36	28.18	✓
LLM	ST-LLM	10.91	35.84	28.25	84.06	✗	4.21	15.77	12.25	28.90	✗
	UrbanGPT	7.38	29.49	36.36	63.63	✓	3.69	13.40	15.83	23.55	✓
Mamba	Mamba	<u>7.17</u>	27.18	<u>25.27</u>	<u>58.53</u>	✓	3.16	10.73	<u>10.75</u>	23.18	✓
	U-Mamba	7.62	<u>25.88</u>	28.47	<u>59.72</u>	✓	3.25	11.36	<u>12.72</u>	<u>22.69</u>	✗
Ours	HealthMamba	6.78	25.24	23.38	56.82	✓	2.98	<u>10.89</u>	10.69	22.24	✓
Texas											
Category	Method	Texas					Florida				
		MAE \downarrow	RMSE \downarrow	MPIW \downarrow	IS \downarrow	COV	MAE \downarrow	RMSE \downarrow	MPIW \downarrow	IS \downarrow	COV
GNN	DCRNN	19.41	135.03	26.16	261.29	✗	140.31	317.69	305.84	648.91	✗
	STGCN	16.79	124.16	57.43	125.01	✗	127.37	291.84	370.57	595.75	✗
	AGCRN	6.54	41.32	16.59	70.71	✗	86.37	210.61	354.67	487.31	✗
	DGCRN	24.41	152.62	41.73	414.77	✗	133.07	307.33	330.68	702.77	✓
	UQGNN	5.40	37.38	17.87	46.08	✓	54.84	132.98	<u>193.39</u>	352.42	✗
Attention	DSTAGNN	10.46	68.95	37.84	72.46	✗	113.71	269.48	339.01	496.03	✗
	ASTGCN	23.71	149.31	28.04	439.70	✗	129.01	316.88	271.01	659.53	✗
Transformer	GluonTS	5.69	38.24	28.39	46.24	✗	91.63	214.03	408.90	531.03	✓
	PatchTST	21.90	145.26	19.07	341.24	✓	127.13	280.98	192.16	640.31	✗
LLM	ST-LLM	6.76	45.72	13.41	66.51	✗	75.37	170.38	258.19	467.20	✓
	UrbanGPT	8.36	51.31	37.10	50.38	✗	<u>44.31</u>	<u>119.76</u>	232.98	<u>330.30</u>	✓
Mamba	Mamba	<u>5.06</u>	<u>35.84</u>	18.64	46.59	✓	64.99	158.42	292.72	429.89	✗
	U-Mamba	<u>5.52</u>	<u>37.88</u>	18.11	<u>45.63</u>	✓	64.58	167.55	238.74	472.80	✗
Ours	HealthMamba	4.62	35.18	<u>18.15</u>	44.50	✓	42.06	118.57	196.62	318.95	✓

trainable parameters, which is moderate compared to GNN-based methods (ranging from 25K for DCRNN to 757K for AGCRN) and similar to Mamba-based baselines (664K–804K). This parameter efficiency, combined with comparable or superior prediction performance, suggests that our architecture effectively utilizes its capacity. The LLM-based methods contain orders of magnitude more parameters (124M for ST-LLM and 6.7B for UrbanGPT), yet do not achieve proportionally better results, highlighting the efficiency of our specialized design for healthcare facility visit prediction.

D.2 Effectiveness of UQ

To further validate the effectiveness of our uncertainty quantification, we employ selective regression [Sokol *et al.*, 2024; Shah *et al.*, 2022], which enables the model to abstain from predictions when confidence is insufficient. As illustrated in Figure 5(a), the MAE curve remains nearly flat when uncertainty quantification is not used, whereas the error consis-

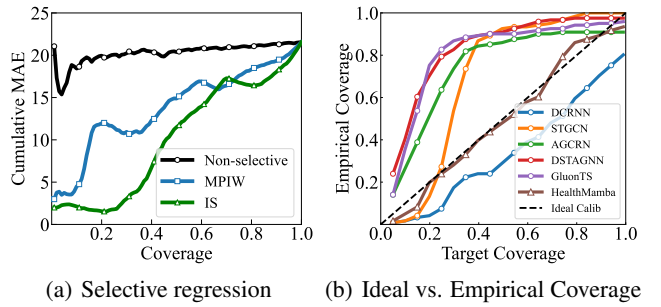


Figure 5: UQ analyses on the California dataset.

tently increases with coverage once uncertainty estimates are incorporated. This confirms that the estimated uncertainty scores are meaningful. Besides, Figure 5(b) shows Health-

Table 6: Prediction performance for 7-day prediction horizon. \downarrow indicates lower is better. The best results are in **bold** and the second-best are underlined. ✓ indicates target coverage ($\geq 90\%$) achieved, while ✗ indicates failure.

Category	Method	California					New York				
		MAE \downarrow	RMSE \downarrow	MPIW \downarrow	IS \downarrow	COV	MAE \downarrow	RMSE \downarrow	MPIW \downarrow	IS \downarrow	COV
GNN	DCRNN	36.85	120.24	90.32	284.13	✗	13.02	42.14	67.44	79.86	✗
	STGCN	39.49	115.13	148.34	250.44	✗	10.86	41.24	45.13	67.22	✗
	AGCRN	21.06	68.45	57.33	160.34	✗	7.82	26.49	21.28	57.81	✗
	DGCRN	34.29	102.85	120.64	252.15	✗	21.25	69.85	23.64	331.79	✗
	UQGNN	12.37	44.25	44.56	94.32	✓	5.57	19.17	19.90	37.89	✗
Attention	DSTAGNN	24.95	67.18	79.25	160.42	✗	10.02	36.14	40.88	60.29	✗
	ASTGCN	56.98	216.34	63.14	910.83	✗	20.32	73.58	18.85	325.64	✗
Transformer	GluonTS	20.47	53.82	108.99	130.23	✗	5.96	19.69	33.43	41.13	✗
	PatchTST	14.98	44.16	74.51	97.39	✗	6.75	24.81	36.84	45.34	✗
LLM	ST-LLM	17.40	57.53	46.58	135.09	✗	6.76	25.29	20.16	46.54	✗
	UrbanGPT	11.78	47.32	59.90	102.39	✗	5.91	21.49	26.06	37.90	✓
Mamba	Mamba	<u>11.44</u>	43.62	<u>41.60</u>	<u>94.05</u>	✗	<u>5.07</u>	17.21	<u>17.70</u>	37.28	✗
	U-Mamba	12.16	<u>41.57</u>	46.90	<u>95.95</u>	✗	5.22	18.23	20.95	<u>36.43</u>	✗
Ours	HealthMamba	10.84	40.71	38.53	91.24	✓	4.77	<u>17.48</u>	17.59	35.71	✓
Texas											
Category	Method	MAE \downarrow	RMSE \downarrow	MPIW \downarrow	IS \downarrow	COV	MAE \downarrow	RMSE \downarrow	MPIW \downarrow	IS \downarrow	COV
		30.95	215.87	41.81	418.45	✗	224.07	508.24	488.72	1039.69	✗
GNN	STGCN	26.81	198.61	91.89	200.04	✗	203.62	467.41	592.82	954.15	✗
	AGCRN	10.44	66.10	26.53	113.17	✗	138.16	337.53	567.45	780.18	✗
	DGCRN	39.01	244.13	66.75	<u>663.69</u>	✗	212.90	492.10	529.22	1124.77	✗
	UQGNN	8.64	59.83	28.58	73.76	✓	87.71	212.79	<u>309.20</u>	564.03	✗
	Attention	16.72	110.33	60.54	115.93	✗	182.00	431.34	542.63	794.37	✗
Transformer	DSTAGNN	37.90	238.89	44.85	703.82	✗	206.36	507.16	433.78	1056.31	✗
	GluonTS	9.09	61.18	45.43	74.03	✗	146.60	342.70	654.24	850.40	✗
LLM	PatchTST	35.00	232.52	30.54	546.73	✗	203.49	449.79	307.46	1025.24	✗
	ST-LLM	10.82	73.23	21.46	106.49	✗	120.65	272.64	412.89	747.83	✗
Mamba	UrbanGPT	13.37	82.13	59.36	80.63	✗	<u>70.92</u>	<u>191.71</u>	372.97	<u>528.76</u>	✓
	Mamba	<u>8.10</u>	<u>57.42</u>	29.82	74.58	✓	104.08	253.69	468.60	688.43	✓
Ours	HealthMamba	7.39	56.28	<u>29.05</u>	71.38	✓	67.30	189.86	314.78	510.60	✓

Mamba achieves the most reliable calibration as its curve is closest to the diagonal line.

D.3 Prediction under Different Horizons

In practice, decision-makers such as governments and public health agencies require healthcare facility visit predictions at different temporal horizons to support effective policy planning. For example, short-term next-day predictions are critical for real-time resource allocation and emergency response, while medium-term (one-week) predictions can inform staffing and intervention design. The ability to provide accurate and reliable predictions across different forecasting horizons is therefore essential for translating predictive models into actionable public health decisions. Hence, we also evaluate HealthMamba across different prediction horizons (1 and 7 days) to assess both short-term and medium-term forecasting capability. As shown in Table 5 and Table 6, our model consistently outperforms baselines across all four

datasets under both horizons.

For short-term (next-day) predictions, HealthMamba achieves the lowest MAE on all datasets, demonstrating superior point prediction accuracy. Notably, our model also maintains the best Interval Score (IS) across most datasets, indicating well-calibrated uncertainty estimates with appropriately narrow prediction intervals. For medium-term (7-day-ahead) predictions, the performance gap between HealthMamba and baselines becomes more pronounced. While all methods experience degradation as the horizon extends, HealthMamba exhibits the most graceful degradation. For instance, on the California dataset, our MAE increases from 6.78 to 10.84, compared to Mamba’s increase from 7.17 to 11.44 with much larger absolute errors. More importantly, HealthMamba is the only method that consistently achieves the target 90% coverage across all datasets for both horizons, validating the robustness of our uncertainty quantification mechanisms.